ATION PAGE

Form Approved
OMB No 0704-0188

AD-A264 598



DATE | 3. REPORT TYPE AND DATES COVERED

4. TITLE AND SUBTITLE
A procedure for a posteriori error estimation for h-p finite element methods

5. FUNDING NUMBERS
DAAL03-89-K-0120

6. AUTHOR(S)
M. Ainsworth and J.T. Oden

7. PERFORMING ORGANIZATION NAME(S) AND ADDRESS(ES)
The University of Texas at Austin
ASE/EM (TICOM)
3500 West Balcones Center Drive
Austin, TX 78759



8. PERFORMING ORGANIZATION REPORT NUMBER

9. SPONSORING/MONITORING AGENCY NAME(S) AND ADDRESS(ES)
U. S. Army Research Office
P. O. Box 12211
Research Triangle Park, NC 27709-2211

10. SPONSORING/MONITORING AGENCY REPORT NUMBER
ARO 26871.8-MA

11. SUPPLEMENTARY NOTES
The view, opinions and/or findings contained in this report are those of the author(s) and should not be construed as an official Department of the Army position, policy, or decision, unless so designated by other documentation.

12a. DISTRIBUTION/AVAILABILITY STATEMENT
Approved for public release; distribution unlimited.

12b. DISTRIBUTION CODE

13. ABSTRACT (Maximum 200 words) A new approach to a posteriori error estimation is outlined which is applicable to general h-p finite element approximations of general classes of boundary value problems. The approach makes use of duality arguments and is based on the element residual method (ERM). In the present exposition, a brief outline of the theoretical foundations of the method is given together with the results of its application to several representative problems. These results show that the approach is applicable to general linearly elliptic systems, including unsymmetrical operators, and that the method is valid for broad classes of linear and non-linear problems.



14. SUBJECT TERMS

15. NUMBER OF PAGES
24

16. PRICE CODE

| 17. SECURITY CLASSIFICATION OF REPORT | 18. SECURITY CLASSIFICATION OF THIS PAGE | 19. SECURITY CLASSIFICATION OF ABSTRACT | 20. LIMITATION OF ABSTRACT |
|---|---|---|---|
| UNCLASSIFIED | UNCLASSIFIED | UNCLASSIFIED | UL |

Computer Methods in Applied Mechanics and Engineering 101 (1992) 73–96
North-Holland

CMA 305

# A procedure for a posteriori error estimation for *h-p* finite element methods

Mark Ainsworth[1] and J. Tinsley Oden
*The University of Texas at Austin, Austin, TX 78712, USA*

Received 14 October 1991

A new approach to a posteriori error estimation is outlined which is applicable to general *h-p* finite element approximations of general classes of boundary value problems. The approach makes use of duality arguments and is based on the element residual method (ERM). Important aspects of the method are that it provides a systematic approach toward deriving element boundary conditions for the ERM; it leads to an upper bound for the global error in an appropriate energy norm, and it is valid for non uniform and irregular *h-p* meshes. In the present exposition, a brief outline of the theoretical foundations of the method is given together with the results of its application to several representative problems. These results show that the approach is applicable to general linearly elliptic systems, including unsymmetrical operators, and that the method is valid for broad classes of linear and non-linear problems.

## 1. Introduction

In a recent paper [1], we developed a general theory for a posteriori error estimation which has the following attributes:

(1) it employs a special variant of the element residual method [1–3];
(2) under mild assumptions, it produces estimates in convenient energy type norms which may not be directly associated with the actual bilinear form of the problem under consideration;
(3) it employs a local duality argument that leads to a guaranteed global upper bound to the error and which generalizes the duality method of Kelly [4];
(4) it is valid for symmetric and unsymmetric operators;
(5) under additional assumptions, the approach can lead to *asymptotically exact* error estimators;
(6) it is well suited to irregular meshes with non-uniform *h-p* finite element approximations and functions independently of the order *p* of the local element shape functions;
(7) it employs a systematic scheme for flux balancing on element boundaries that substantially increases the quality of the local and global effectivity indices.

*Correspondence to:* Mark Ainsworth, Texas Institute for Computational Mechanics, WRW 305, The University of Texas, Austin, TX 78712, USA.
[1] On leave from Mathematics Department, Leicester University, Leicester, UK.

The theory generalizes previous work on the ERM. In particular, for the special case of linear triangles ($p = 1$), the conjecture made by Bank and Weiser [2] is confirmed: that a certain variant of the ERM always provides an upper bound on the error.

Our purpose in the present paper is to briefly outline the principal features of the theory in connection with a simple model elliptic boundary value problem and to focus on issues of implementation. The robustness and generality of the method is demonstrated by some applications including elliptic systems and unsymmetrical problems. The applicability of the method to arbitrary $h$-$p$ meshes is also illustrated. In particular, it is demonstrated that the method yields very good local estimates both for meshes with odd and with even order shape functions on neighboring elements, in contrast to other techniques proposed in recent literature.

## 2. Theoretical foundations

### 2.1. Model problem

For clarity, we begin by considering a simple model elliptic boundary value problem in two dimensions: Find $u = u(x, y)$ such that

$$\begin{aligned} &-\nabla\cdot(a\nabla u) + \boldsymbol{b}\cdot\nabla u + cu = f \quad \text{in } \Omega\,, \\ &a\frac{\partial u}{\partial n} = g \quad \text{on } \Gamma_N\,, \qquad u = 0 \quad \text{on } \Gamma_D\,, \end{aligned} \tag{1}$$

where $\Omega$ is a connected Lipschitzian domain in $\mathbb{R}^2$ with boundary $\partial\Omega = \overline{\Gamma_N \cap \Gamma_D}$. In (1), the coefficients $a$, $\boldsymbol{b}$, $c$ and data $f$, $g$ are assumed to be such that $u$ exists, is unique, is continuous on the interior of $\Omega$ and depends continuously on the data in appropriate norms. The weak form of (1) is as follows: Find $u \in \mathcal{V}$ such that

$$B(u, v) = L(v) \quad \forall v \in \mathcal{V}\,, \tag{2}$$

where

$$\mathcal{V} = \{v \in H^1(\Omega)\colon \gamma v = 0 \text{ on } \Gamma_D\} \tag{3}$$

and $B : \mathcal{V} \times \mathcal{V} \to \mathbb{R}$, $L : \mathcal{V} \to \mathbb{R}$ are the forms

$$B(u, v) = \int_\Omega (a\nabla u\cdot\nabla v + v\boldsymbol{b}\cdot\nabla u + cuv)\,\mathrm{d}\boldsymbol{x} \tag{4}$$

and

$$L(v) = \int_\Omega fv\,\mathrm{d}\boldsymbol{x} + \int_{\Gamma_N} gv\,\mathrm{d}s\,. \tag{5}$$

### 2.2. Partitioning

We next introduce a partitioning $\mathcal{P}$ of $\Omega$ into $N = N(\mathcal{P})$ subdomains (finite elements) $\Omega_k$ where $\bar{\Omega} = \bigcup \bar{\Omega}_k$ and construct on $\mathcal{P}$ a space $\hat{\mathcal{V}} \subset \mathcal{V}$ of piecewise polynomial functions. The space $\hat{\mathcal{V}}$ could include arbitrary $h$-$p$ finite element approximations of the type discussed in [5].

Following standard finite element procedures, we suppose that a function $\hat{u} \in \mathcal{V}$ is obtained which represents, in some sense, an approximation of the solution $u$ of (1). Our goal is to use the available information to calculate an estimate of the error

$$e = u - \hat{u}$$

in an appropriate norm.

With regard to the partition $\mathcal{P}$, we introduce the following notation: $B_K$, $L_K$ are localizations of the forms in (4) and (5),

$$B_K(u, v) = \int_{\Omega_K} (a\nabla u \cdot \nabla v + v\boldsymbol{b} \cdot \nabla u + cuv)\, \mathrm{d}\boldsymbol{x}\,, \tag{6}$$

$$B(u, v) = \sum_{K=1}^{N} B_K(u, v)\,, \tag{7}$$

$$L_K(v) = \int_{\Omega_K} fv\, \mathrm{d}\boldsymbol{x} + \int_{\Gamma_N \cap \partial\Omega_K} gv\, \mathrm{d}s\,, \tag{8}$$

$$L(v) = \sum_{K=1}^{N} L_K(v)\,, \tag{9}$$

for $u, v \in \mathcal{V}$. Further $\mathcal{V}_K$ is a local subspace of $\mathcal{V}$, with

$$\mathcal{V} = \bigoplus_{K=1}^{N} \mathcal{V}_K\,. \tag{10}$$

There now arises the issue of the norm in which we shall measure the error $e$. For this purpose, we introduce a *symmetric*, *positive definite* bilinear form $a : \mathcal{V} \times \mathcal{V} \to \mathbb{R}$.

$$a(u, v) = \int_{\Omega} (\bar{a}\nabla u \cdot \nabla v + \bar{c}uv)\, \mathrm{d}\boldsymbol{x}\,, \tag{11}$$

where $\bar{a}$ and $\bar{c}$ are constants which are arbitrary except for the requirement that the original bilinear form $B(\cdot\,, \cdot)$ of (4) is coercive with respect to the norm induced by $a(\cdot\,, \cdot)$. That is,

$$\sup_{v \in \mathcal{V}} \frac{|B(u, v)|}{\|v\|_a} \geqslant \beta \|u\|_a\,, \quad \forall u \in \mathcal{V}\,. \tag{12}$$

where $\beta > 0$ is a constant, and

$$\|v\|_a = \sqrt{a(v, v)}\,. \tag{13}$$

In addition, we write

$$a(u, v) = \sum_{K=1}^{N} a_K(u, v)\,, \tag{14}$$

$$a_K(u, v) = \int_{\Omega_K} (a\nabla u \cdot \nabla v + \bar{c}uv)\, \mathrm{d}\boldsymbol{x}\,, \tag{15}$$

$$\|v\|_{\mathscr{E},K}^2 = a_K(v, v)\,, \tag{16}$$

$$\|v\|_{\mathscr{E}} = \sum_{K=1}^{N} \|v\|_{\mathscr{E},K}^2\,. \tag{17}$$

We also introduce the averaged local flux

$$\langle \boldsymbol{n}_K \cdot a\nabla\hat{u}\rangle(s) = \boldsymbol{n}_K \cdot [(1 - \alpha_{KJ}(s))a\nabla\hat{u}|_K + \alpha_{KJ}(s)a\nabla\hat{u}|_J]\,, \tag{18}$$

where $s$ is a point on the interelement boundary $\Gamma_{KJ} = \partial\Omega_K \cap \partial\Omega_J$ shared by neighboring elements, $\boldsymbol{n}_K$ is the unit vector exterior and normal to $\partial\Omega_K$, and $\alpha_{KJ}$ is a linear function associated with edge $\Gamma_{KJ}$.

With this notation now established, we consider the following *local problem*: Find $\phi_K \in \mathscr{E}_K$ such that

$$a_K(\phi_K, w) = L_K(w) - B_K(\hat{u}, w) + \oint_{\partial\Omega_K} w\langle \boldsymbol{n}_K \cdot a\nabla\hat{u}\rangle(s)\, \mathrm{d}s\,, \quad w \in \mathscr{E}_K\,. \tag{19}$$

Equation (19) characterizes the local problem providing the basis for the error residual method corresponding to the norm $\|\cdot\|_{\mathscr{E}}$. The significance of (19) is embodied in the following theorem.

*THEOREM 1. Let $\phi_K$ be the solution of the local problem (19) corresponding to the element $\Omega_K$. Then the functions $\alpha_{KJ}$ of (18) can be chosen so that*

$$\|e\|_{\mathscr{E}}^2 \leq \frac{1}{\beta^2} \sum_{K=1}^{N} \|\phi_K\|_{\mathscr{E},K}^2\,, \tag{20}$$

*where $\beta$ is the constant appearing in (12).*

PROOF. See [1, 6].

*REMARK 1.* In the case in which the bilinear from $B(\cdot, \cdot)$ is symmetric and positive definite, we can take $a(\cdot, \cdot) = B(\cdot, \cdot)$. Then the constant $\beta = 1$ and the norm $\|\cdot\|_{\mathscr{E}}$ reduces to the standard energy norm.

*REMARK 2.* The introduction of the symmetric form $a(\cdot, \cdot)$ is equivalent to symmetrizing the problem [7].

*REMARK 3.* The conditions on the approximate solution $\hat{u}$ (that $\hat{u} \in \mathscr{E}$) can be weakened considerably. Let $\psi$ be a standard degree 1 basis function (a pyramid function) associated with a regular node in $\mathscr{P}$. Then we need only require that $\hat{u} \in C^0(\Omega) \cap H^2(\mathscr{P}) \cap \mathscr{E}$ and

$$B(\hat{u}, \psi) = L(\psi)\,. \tag{21}$$

That is, $\hat{u}$ need only satisfy an orthogonality condition with respect to the lowest degree basis function.

*REMARK 4.* Let $h_K = \mathrm{diam}(\Omega_K)$ and suppose that

$$|B(u, v)| \leq M\|u\|_1 \|v\|_1, \quad \forall u, v \in \mathcal{V}. \tag{22}$$

As an additional assumption, suppose that the following condition holds:

$$\sum_{K=1}^{N} h_K \oint_{\partial\Omega_K \cap \partial\Omega} [\langle \boldsymbol{n}_K \cdot a\nabla\hat{u}\rangle - \boldsymbol{n}_K \cdot a\nabla u]^2 \, \mathrm{d}s \leq \rho\|e\|_1^2, \tag{23}$$

where $\rho = \rho(h, p)$ is a constant possibly depending on the mesh parameters $h$ and $p$. Then it can be shown [1, 2] that

$$\sum_{K=1}^{N} \|\phi_K\|_{1,K}^2 \leq M\{1 + \mathrm{O}(\bar{h}) + C\rho\}\|e\|_1^2, \tag{24}$$

where $\bar{h} = \max_K h_K$. Then we have

$$\beta\|e\|_1^2 \leq \sum_{K=1}^{N} \|\phi_K\|_{1,K}^2 \leq \hat{M}\|e\|_1^2, \tag{25}$$

where $\hat{M}$ depends on $M$, $\bar{h}$ and $\rho$. This result establishes the equivalence of the global a posteriori error estimate to the true error. Moreover, if $\rho \to 0$ as $\bar{h} \to 0$ then we have $\hat{M} \to M$. This shows that the constants appearing in (25) are asymptotically optimal. In the case of $B(\cdot, \cdot)$ symmetric and positive definite, we have asymptotic exactness of the error estimator.

## 3. Implementation

The actual computation of the error estimator may be thought of as consisting of two distinct stages:

(a) the calculation of the linear splitting function $\alpha_{KJ}$ used in (18) to obtain the boundary conditions for the local problem (19),

(b) the (approximation of) the solution of the local problem (19).

The fundamental criterion determining the choice of flux splittings used in the average (18), is the following:

$$B_K(\hat{u}, 1) = L_K(1) + \int_{\partial K \cap \Gamma_N} \langle \boldsymbol{n}_K \cdot a\nabla\hat{u}\rangle(s) \, \mathrm{d}s. \tag{26}$$

A simple physical interpretation of (26) is seen in the special case $a(\boldsymbol{x}) \equiv 1$, $\boldsymbol{b}(\boldsymbol{x}) \equiv 0$ and $c(\boldsymbol{x}) \equiv 0$. For this situation (26) becomes

$$0 = \int_K f(\boldsymbol{x}) \, \mathrm{d}\boldsymbol{x} + \int_{\partial K \cap \Gamma_N} g(s) \, \mathrm{d}s + \int_{\partial K \cap \Gamma_N} \langle \boldsymbol{n}_K \cdot a\nabla\hat{u}\rangle(s) \, \mathrm{d}s. \tag{27}$$

The condition (27) proclaims that the data for the local problem (19) is in equilibrium, or that the fluxes have been equilibrated.

Kelly [4] used this same criterion to determine flux splittings in the case of piecewise bilinear finite element approximation of Poisson's equation in two dimensions. Our approach, while related to Kelly's, differs significantly in several ways. The splittings used in our algorithm are linear functions, as opposed to constants; our splittings can be obtained using only *local* computations rather than applying a *global* optimization procedure; and, under mild assumptions, achieve the equilibration exactly (subject to rounding error) and are applicable to general linear elliptic systems of second order partial differential equations. In addition, our approach applies to general *h-p* finite element approximations on irregular meshes, with non-uniform $p$ and is valid for triangular elements, quadrilateral elements or indeed combinations of the two. Importantly, our approach applies equally well to one, two or three dimensions.

### 3.1. *The flux splitting algorithm*

The complete details involved in deriving the algorithm to be presented can be found in [8]. Here, we restrict ourselves to the bare essentials necessary to implement the algorithm.

A key role in the algorithm is played by the degree one basis functions (that is, the pyramid functions associated with the regular nodes in the partition). Denote the regular nodes by $A, B, \ldots$ and let $\psi_A$ denote the pyramid function associated with node $A$ (scaled so that $\psi_A = 1$ at node $A$).

The computations are localized using the patches of elements over which the functions $\psi_A$ have non-zero values. For ease of notation, we suppose elements $\Omega_1, \Omega_2, \ldots, \Omega_N$ constitute the patch $S_A$ of elements on which $\psi_A$ does not vanish. Some examples of possible patches are shown in Figs. 1–3.

Associated with each patch $S_A$ is a matrix $T_A$. The matrix depends only on the *topology* of the patch $S_A$ and not on the geometry. For this reason we refer to $T_A$ as the topology matrix for the patch. $T_A$ is a square matrix of size $N \times N$, where $N$ is the number of elements in the patch. Therefore, $T_A$ are typically small matrices whose sizes do not increase as the partition is refined. The entries of $T_A$ are given by

$$T_A = \begin{bmatrix} 2 & 0 & -1 & -1 \\ 0 & 2 & -1 & -1 \\ -1 & -1 & 2 & 0 \\ -1 & -1 & 0 & 2 \end{bmatrix} \quad \text{(Fig. 1)}, \tag{28}$$

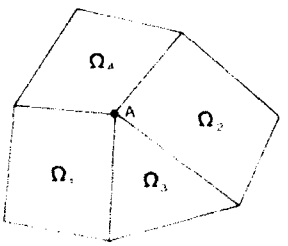


Fig. 1. Topology matrix for interior node on regular mesh.

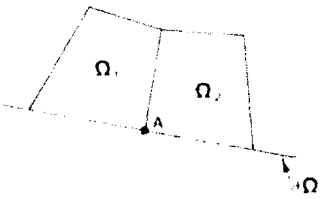


Fig. 2. Topology matrix for boundary node.

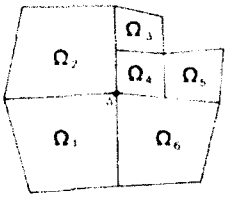


Fig. 3. Topology matrix for interior node on 1-irregular mesh.

$$T_A = \begin{bmatrix} 1 & -1 \\ -1 & 1 \end{bmatrix} \quad \text{(Fig. 2)}, \tag{29}$$

$$T_A = \begin{bmatrix} 2 & -1 & 0 & 0 & 0 & -1 \\ -1 & 3 & -1 & -1 & 0 & 0 \\ 0 & -1 & 2 & -1 & 0 & 0 \\ 0 & -1 & -1 & 4 & -1 & -1 \\ 0 & 0 & 0 & -1 & 2 & -1 \\ -1 & 0 & 0 & -1 & -1 & 3 \end{bmatrix} \quad \text{(Fig. 3)}, \tag{30}$$

$$(T_A)_{ij} = \begin{cases} C_i, & \text{if } j = i, \\ -1, & \text{if } \Omega_i \text{ and } \Omega_j \text{ are neighbours in the patch}, \\ 0, & \text{otherwise}, \end{cases} \tag{31}$$

where $C_i$ is the number of elements in the patch which share an edge with element $\Omega_i$. Some examples of topology matrices for various types of patch in two dimensions are shown in Figs. 1–3.

The singular matrix $T_A$ is then modified by adding 1 to every entry, thereby giving a new matrix $\hat{T}_A$ with entries

$$(\hat{T}_A)_{ij} = \begin{cases} C_i + 1, & \text{if } j = i, \\ 0, & \text{if } \Omega_i \text{ and } \Omega_j \text{ are neighbours in the patch}, \\ 1, & \text{otherwise}, \end{cases} \tag{32}$$

where $C_i$ is as before. It may be shown [8] that $\hat{T}_A$ is non-singular. In fact it is symmetric, positive definite and consequently simple to invert numerically (using, for example, an LU factorization).

Define the $N$-vector $\boldsymbol{b}_A$ with entries

$$(\boldsymbol{b}_A)_K = L_K(\psi_A) - B_K(\hat{u}, \psi_A) + \int_{\partial K - \partial\Omega} \psi_A(s) \langle \boldsymbol{n}_K \cdot a\nabla\hat{u} \rangle_{1,2}\, \mathrm{d}s, \tag{33}$$

where

$$\langle \boldsymbol{n}_K \cdot a\nabla\hat{u} \rangle_{1,2} = \tfrac{1}{2}\boldsymbol{n}_K \cdot [a\nabla\hat{u}|_K + a\nabla\hat{u}|_J], \quad s \in \Gamma_{KJ}. \tag{34}$$

Furthermore, for every interelement edge $\Gamma_{KJ}$ within the patch define

$$\rho_{KJ,A} = -\int_{\Gamma_{KJ}} \psi_A(s) [\![ \boldsymbol{n} \cdot a\nabla\hat{u} ]\!]\, \mathrm{d}s, \tag{35}$$

where

$$[\![ \boldsymbol{n} \cdot a\nabla\hat{u} ]\!] = \boldsymbol{n}_K \cdot a\nabla\hat{u}|_K + \boldsymbol{n}_J \cdot a\nabla\hat{u}|_J, \quad s \in \Gamma_{KJ}. \tag{36}$$

Having calculated these various quantities, a set of *constants* $\alpha_{KL}^{1}$ is computed using the procedure outlined in Fig. 4. The case when $\rho_{KL,A}$ vanishes requires a little extra care, details of which can be found in [8].

The procedure in Fig. 4 is applied to every regular node in the mesh. The actual flux splitting $\alpha_{KL}$ used in (18) is then given by

$$\alpha_{KL}(s) = \sum_{A} \alpha_{KL,A} \psi_A(s), \quad s \in \Gamma_{KL}. \tag{37}$$

Most of the terms in this summation vanish due to $\psi_A$ having non-zero values on a small number of edges. For example, in the case of regular meshes, only two terms in the summation are non-zero, namely those corresponding to the two nodes forming the endpoints of the edge $\Gamma_{KL}$, i.e. $\alpha_{KL}$ is then the linear function which interpolates to $\alpha_{KL,A}$ and $\alpha_{KL,B}$ at the endpoints of the edge. In the case of irregular meshes the situation is more complicated with at most three non-zero terms appearing in the sum.

It can be shown [8] that, with this choice of splitting, the condition (26) is satisfied. The process described may appear elaborate. However, the computational work entailed is rather small by comparison with the cost of performing other standard tasks in the finite element method. In [8], an operation count shows that the process is of optimal order, increasing only linearly with the number of elements in the partition.

### 3.2. *Approximation of local problems*

The approximation of the local problem (19) is performed by means of a Galerkin method using a particular set of trial functions. Here, we shall describe the procedure we use for quadrilateral elements.

Let $\{P_n(x)\}$ denote the usual Legendre polynomials on $[-1, 1]$. It will be necessary to be able to compute the values of the polynomials themselves and their derivatives efficiently. Unfortunately, in many textbooks it is suggested that these quantities be calculated directly from the expansion in terms of powers of $x$. This approach is not only unnecessarily expensive

```
for each regular node A do
 begin
  calculate T̂_A;
  calculate an LU factorization L_A U_A = T̂_A;
  for every element K ∈ S_A do
   begin
    calculate b_{K,A};
    calculate ρ_{KL,A}
   end;
  solve L_A U_A λ_A = ω_A;
  for every interelement edge Γ_KL in the patch do
   begin
    α_{KL,A} = ½ + (λ_{K,A} − λ_{L,A}) / ρ_{KL,A}
   end
  end;
```

Fig. 4. Pseudo-code of flux splitting algorithm.

but leads to catastrophic build up of round-off errors. Therefore, we use the three term recurrence relations. Thus, for some fixed value of $x$, we calculate $P_n(x)$ and $P_n'(x)$ as follows:

$$P_0(x) = 1\,, \qquad P_1(x) = x\,, \tag{38}$$

$$P_{k+1}(x) = \frac{2k+1}{k+1}\,xP_k(x) - \frac{k}{k+1}\,P_{k-1}(x)\,, \quad k = 1\,,$$

and

$$P_0'(x) = 0\,, \qquad P_1'(x) = 1\,, \tag{38}$$

$$P_{k+1}'(x) = \frac{2k+1}{k}\,xP_k'(x) - \frac{k+1}{k}\,P_{k-1}'(x)\,, \quad k = 1\,,$$

To calculate the values of $P_n(x)$ and $P_n'(x)$ in this way requires only order $n$ operations. Moreover, as a byproduct, one also obtains the values of all the lower order polynomials and their derivatives at no extra expense.

The values of $P_0(x), \ldots, P_n(x)$ and $P_0'(x), \ldots, P_n'(x)$ are then used to compute the functions $\chi_0(x), \ldots, \chi_n(x)$ and $\chi_0'(x), \ldots, \chi_n'(x)$ given by

$$\chi_0(x) = \sqrt{\frac{1}{2}}\,P_0(x)\,, \qquad \chi_1(x) = \sqrt{\frac{1}{2}}\,P_1(x)\,, \qquad \chi_2(x) = \frac{1}{3}\sqrt{\frac{3}{2}}\,P_2(x)\,,$$

$$\chi_k(x) = \frac{1}{k(k-1)}\sqrt{\frac{2k-1}{2}}\,(x^2-1)P_{k-1}'(x)\,, \quad k = 3, \ldots, n\,, \tag{40}$$

and

$$\chi_0'(x) = 0\,, \qquad \chi_1'(x) = \sqrt{\frac{1}{2}}\,P_0(x)\,, \qquad \chi_2'(x) = \sqrt{\frac{3}{2}}\,P_1(x)\,,$$

$$\chi_k'(x) = \sqrt{\frac{2k-1}{2}}\,P_{k-1}(x)\,, \quad k = 3, \ldots, n\,, \tag{41}$$

Let $\hat{\Omega} = [-1, 1] \times [-1, 1]$ denote the usual reference element. The trial functions will be defined on $\hat{\Omega}$. For simplicity, assume that the finite element approximation $\hat{u}$ is a complete polynomial of degree $p$ on the element under consideration. Let $q > 0$ be an integer; then we define the space $V^{p,q}(\hat{\Omega})$ by

$$V^{p,q}(\hat{\Omega}) = \{\chi_j(\xi)\chi_k(\eta) \mid 0 \leq j,k \leq p+q \text{ and at least one of } j, k > p\}\,. \tag{42}$$

It is seen that $\dim(V^{p,q}) = (p+q+1)^2 - (p+1)^2$. The index $q$ controls the number of increments in the polynomial degree of the space and may be used to increase the dimension of the space.

The local approximation space is then taken to be $\tilde{\mathcal{T}}_K = \mathcal{T}_K \cap V^{p,q}(\Omega_K)$. The discretized version of the local problem (19) is: Find $\tilde{\phi}_K \in \tilde{\mathcal{T}}_K$ such that

$$a_K(\tilde{\phi}_K, w) = L_K(w) - B_K(\hat{u}, w) + \oint_{\partial\Omega_K} w\langle \boldsymbol{n}_K \cdot a\nabla\hat{u}\rangle(s)\,ds \quad \forall w \in \tilde{\mathcal{T}}_K\,. \tag{43}$$

Owing to the above assumptions and the construction of the local space, this problem always has a unique solution.

## 4. Numerical examples

In this section we present three examples to illustrate the performance of the algorithm.

In order to compare the estimated error with the true error it is necessary to accurately calculate the true error over each element. In all our examples, the true error is computed using an algorithm which approximates the integral using first a single subdomain and then subdivides the region of integration into four subdomains and approximates the integral over the four subregions. Two estimates are thus obtained for the true value of the integral. If the difference in these two estimates is less than 1% relative error, then the approximation is accepted. Otherwise, the element is further subdivided into 16 regions and so on until agreement between consecutive approximations is obtained to less than 1% relative error.

### 4.1. Symmetric elliptic operator with smooth solution

The problem we consider is: Find $u$ such that

$$-\Delta u + u = 0 \quad \text{in } \Omega\,, \tag{44}$$

subject to the boundary conditions

$$\begin{aligned} &u(0, y) = (e^{\sqrt{1+\sigma^2}} - 1)\sin \sigma y\,, \quad 0 \leqslant y \leqslant 1/2\,, \\ &u(x, 0) = u(x, 1/2) = 0\,, \quad 0 \leqslant x \leqslant 1/2\,, \qquad \frac{\partial u}{\partial n} = 0\,, \quad x = 1/2,\ 0 \leqslant y \leqslant 1/2\,, \end{aligned} \tag{45}$$

where $\sigma = 2\pi$. The geometry of the domain $\Omega$ and the boundary conditions applied are shown in Fig. 5.

The true solution is given by

$$u(x, y) = (\exp[(x-1)\sqrt{1+\sigma^2}] - \exp(-x\sqrt{1+\sigma^2}))\sin \sigma y\,. \tag{46}$$

In this case, we have

$$B(u, v) = \int_\Omega (\nabla u \cdot \nabla v + uv)\,\mathrm{d}x \tag{47}$$

and we choose $a(u, v) = B(u, v)$. Theorem 1 predicts that we will obtain guaranteed upper bounds on the true error measured in the energy norm defined by $B(\cdot\,, \cdot)$, provided that equilibration of the fluxes is achieved.

The problem is solved using uniform meshes of quadrilateral elements with uniform polynomial degree. The local problems are approximated using an increment $q = 2$ in the local space. That is, a degree $p$ finite element approximation is analyzed using the space $V^{p,p+2}$. In each case, the equilibration procedure is able to reduce the lack of equilibration to the level of round off error on virtually every element in the partition.

Table 1 contains the results obtained for finite element approximations of degree 1–4 on

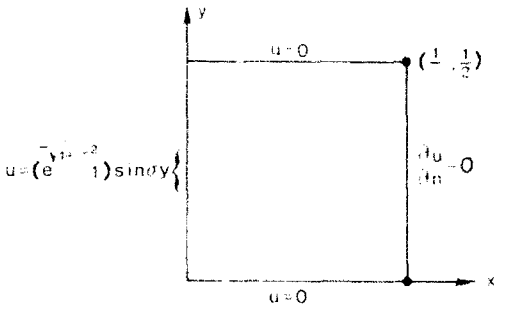


Fig. 5. Geometry and boundary conditions for smooth model problem.

Table 1
Global effectivity indices for model problem with smooth solution

| Degree ($p$) | Number of elements | | |
|---|---|---|---|
| | 16 | 64 | 128 |
| 1 | 1.0129099 | 1.0033555 | 1.0009907 |
| 2 | 1.0007872 | 1.0002019 | 1.0000360 |
| 3 | 1.0000265 | 1.0000098 | 1.0000031 |
| 4 | 1.0000237 | 1.0000120 | 1.0000050 |

meshes containing 16, 64 and 128 elements. The quantity shown in the table is the *effectivity index* (the ratio of the estimated error to the true error). Theorem 1 predicts that the effectivity index be greater than unity. This prediction is borne out by the results shown in Table 1.

### 4.2. *Cracked panel problem*

Consider the problem: Find $u$ such that

$$-\Delta u = 0 \quad \text{in } \Omega\,, \tag{48}$$

subject to the boundary conditions

$$u(r, \pi) = 0\,, \quad 0 < r < 1\,, \qquad \partial u/\partial n = 0\,, \quad 0 < r < 1\,,\ \theta = 0\,, \tag{49}$$

with $u(r, \theta) = r^{\frac{1}{2}} \cos \frac{1}{2}\theta$ on the remaining portion of the boundary. The geometry of the domain $\Omega$ is shown in Fig. 6.

The true solution is given by

$$u(r, \theta) = r^{\frac{1}{2}} \cos \tfrac{1}{2}\theta\,. \tag{50}$$

The problem is the analogue of a cracked panel problem in linear elasticity, with a singularity

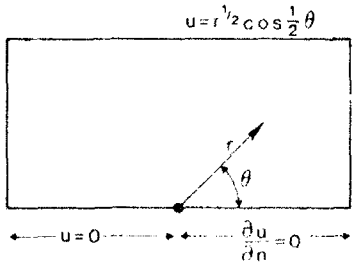


Fig. 6. Geometry and boundary conditions for cracked panel problem.

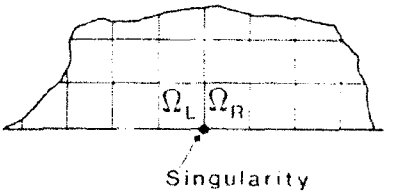


Fig. 7. Position of elements adjacent to singularity in cracked panel.

at the origin. In this case, we have

$$B(u, v) = \int_{\Omega} \nabla u \cdot \nabla v \, \mathrm{d}x \tag{51}$$

and we take $a(u, v) = B(u, v)$. Theorem 1 again predicts that we will obtain upper bounds on the true error, provided that we equilibrate the fluxes.

In analyzing this problem, some care must be taken with the approximation of the local problems. Theorem 1 assumes that the local problems are solved exactly, which is not the case in practice. Therefore, for the purposes of illustrating the theory, a sequence of approximations to the true solution of the local problem is obtained by incrementing $q$. That is to say, we compute a sequence of approximations using the spaces

$$V^{p,q+1} \subset V^{p,q+2} \subset V^{p,q+3} \subset \cdots$$

until the difference in the norm of the approximation is sufficiently small.

One other feature of this particular example is the difficulty in estimating the error in elements adjacent to the singular point. Our theory makes no promises concerning the effectivity of the estimator in a single element. However, we present results showing the estimated and the true error in the elements adjacent to the singularity $\Omega_1$ and $\Omega_R$ (see Fig. 7).

Tables 2–4 contain results of estimating the error in the approximation obtained using a uniform mesh of 32 quadrilateral elements with uniform polynomial degree 1. Five increments in the local approximation space are needed before agreement is obtained. For purposes of comparison, we also give the results obtained when no equilibration or balancing of fluxes is performed (instead, a simple averaging is applied).

Tables 2 and 3 contain the error estimates in the elements adjacent to the singularity $\Omega_1$ and $\Omega_R$. The estimate of the error obtained when equilibration of fluxes is performed is superior to the estimate obtained using a simple averaging. Table 4 contains the global estimates of the error. It is seen that it is necessary to approximate the local problems accurately if one is to obtain the upper bound proclaimed by Theorem 1.

Table 2
Effect of solving local problem with increasing accuracy on the estimates of local error in element $\Omega_1$ for cracked panel ($p = 1$, 32 elements)

| Number of increments | Estimated local error | | Local effectivity index | |
|---|---|---|---|---|
| | With balancing | Without balancing | With balancing | Without balancing |
| 1 | 0.132644 | 0.635051(−1) | 0.973984 | 0.466308 |
| 2 | 0.132644 | 0.635051(−1) | 0.973984 | 0.466308 |
| 3 | 0.150311 | 0.679112(−1) | 1.103710 | 0.498661 |
| 4 | 0.153503 | 0.686562(−1) | 1.127149 | 0.504132 |
| 5 | 0.154516 | 0.689176(−1) | 1.134587 | 0.506051 |
| True value | 0.136187 | 0.136187(+0) | 1.000000 | 1.000000 |

Table 3
Effect of solving local problem with increasing accuracy on the estimates of local error in element $\Omega_R$ for cracked panel ($p = 1, 32$ elements)

| Number of increments | Estimated local error | | Local effectivity index | |
|---|---|---|---|---|
| | With balancing | Without balancing | With balancing | Without balancing |
| 1 | 0.109140 | 0.183891 | 0.847281 | 1.427592 |
| 2 | 0.109140 | 0.183891 | 0.847281 | 1.427592 |
| 3 | 0.112848 | 0.184056 | 0.876067 | 1.428873 |
| 4 | 0.113189 | 0.184062 | 0.878715 | 1.428920 |
| 5 | 0.113216 | 0.184062 | 0.878924 | 1.428920 |
| True value | 0.128812 | 0.128812 | 1.000000 | 1.000000 |

Table 4
Effect of solving local problem with increasing accuracy on the estimates of global error for cracked panel ($p = 1, 32$ elements)

| Number of increments | Estimated global error | | Global effectivity index | |
|---|---|---|---|---|
| | With balancing | Without balancing | With balancing | Without balancing |
| 1 | 0.183726 | 0.206899 | 0.921963 | 1.038248 |
| 2 | 0.183726 | 0.206899 | 0.921963 | 1.038248 |
| 3 | 0.199198 | 0.208800 | 0.999604 | 1.047788 |
| 4 | 0.201876 | 0.209060 | 1.013042 | 1.049092 |
| 5 | 0.202664 | 0.209149 | 1.016997 | 1.049539 |
| True value | 0.199277 | 0.199277 | 1.000000 | 1.000000 |

Table 5
Effect of solving local problem with increasing accuracy on the estimates of local error in element $\Omega_1$ for cracked panel ($p = 1, 128$ elements)

| Number of increments | Estimated local error | | Local effectivity index | |
|---|---|---|---|---|
| | With balancing | Without balancing | With balancing | Without balancing |
| 1 | 0.927019(−1) | 0.443847(−1) | 0.959405 | 0.459353 |
| 2 | 0.927019(−1) | 0.443847(−1) | 0.959405 | 0.459353 |
| 3 | 0.105048(0) | 0.474636(−1) | 1.087179 | 0.491218 |
| 4 | 0.107279(0) | 0.479842(−1) | 1.110268 | 0.496605 |
| 5 | 0.107987(0) | 0.481669(−1) | 1.117596 | 0.498496 |
| True value | 0.966244(−1) | 0.966244(−1) | 1.000000 | 1.000000 |

Tables 5–7 show the corresponding results obtained when the mesh is refined uniformly to 128 elements of degree one. The results obtained are similar to the case of 32 elements. Tables 8–10 contain the results obtained when the degree of the elements is increased uniformly to degree 2 on 32 elements. Once again, the results show the superiority of the estimate obtained

Table 6
Effect of solving local problem with increasing accuracy on the estimates of local error in element $\Omega_K$ for cracked panel ($p = 1$, 128 elements)

| Number of increments | Estimated local error | | Local effectivity index | |
|---|---|---|---|---|
| | With balancing | Without balancing | With balancing | Without balancing |
| 1 | 0.762753(−1) | 0.128522(0) | 0.855679 | 1.441798 |
| 2 | 0.762753(−1) | 0.128522(0) | 0.855679 | 1.441798 |
| 3 | 0.788666(−1) | 0.128637(0) | 0.884749 | 1.443088 |
| 4 | 0.791049(−1) | 0.128641(0) | 0.887422 | 1.443133 |
| 5 | 0.791235(−1) | 0.128642(0) | 0.887631 | 1.443144 |
| True value | 0.891401(−1) | 0.891401(−1) | 1.000000 | 1.000000 |

Table 7
Effect of solving local problem with increasing accuracy on the estimates of global error for cracked panel ($p = 1$, 128 elements)

| Number of increments | Estimated global error | | Global effectivity index | |
|---|---|---|---|---|
| | With balancing | Without balancing | With balancing | Without balancing |
| 1 | 0.129397 | 0.145495 | 0.918497 | 1.032766 |
| 2 | 0.129397 | 0.145495 | 0.918497 | 1.032766 |
| 3 | 0.140126 | 0.146813 | 0.994655 | 1.042121 |
| 4 | 0.141983 | 0.146992 | 1.007836 | 1.043392 |
| 5 | 0.142531 | 0.147053 | 1.011726 | 1.043825 |
| True value | 0.140879 | 0.140879 | 1.000000 | 1.000000 |

Table 8
Effect of solving local problem with increasing accuracy on the estimates of local error in element $\Omega_1$ for cracked panel ($p = 2$, 32 elements)

| Number of increments | Estimated local error | | Local effectivity index | |
|---|---|---|---|---|
| | With balancing | Without balancing | With balancing | Without balancing |
| 1 | 0.779887(−1) | 0.405007(−1) | 0.971502 | 0.504516 |
| 2 | 0.877218(−1) | 0.443006(−1) | 1.092747 | 0.551851 |
| 3 | 0.916439(−1) | 0.457423(−1) | 1.141605 | 0.569810 |
| 4 | 0.924515(−1) | 0.466069(−1) | 1.151665 | 0.580580 |
| 5 | 0.932539(−1) | 0.463873(−1) | 1.161660 | 0.577845 |
| True value | 0.802764(−1) | 0.802764(−1) | 1.000000 | 1.000000 |

using equilibrated fluxes. In each case, the result of Theorem 1 is verified, although it is necessary to solve the local problems very accurately.

### 4.3. *Unsymmetric elliptic system*

As a final example, we consider the unsymmetric elliptic system with non-constant convection given by: Find $u_1$, $u_2$ such that

Table 9
Effect of solving local problem with increasing accuracy on the estimates of local error in element $\Omega_8$ for cracked panel ($p = 2$, 32 elements)

| Number of increments | Estimated local error | | Local effectivity index | |
|---|---|---|---|---|
| | With balancing | Without balancing | With balancing | Without balancing |
| 1 | 0.532473(−1) | 0.665535(−1) | 0.686000 | 0.857427 |
| 2 | 0.613689(−1) | 0.717056(−1) | 0.790633 | 0.923803 |
| 3 | 0.628189(−1) | 0.848990(−1) | 0.809313 | 1.093777 |
| 4 | 0.644079(−1) | 0.876593(−1) | 0.829785 | 1.129339 |
| 5 | 0.648299(−1) | 0.912130(−1) | 0.835222 | 1.175122 |
| True value | 0.776200(−1) | 0.776200(−1) | 1.000000 | 1.000000 |

Table 10
Effect of solving local problem with increasing accuracy on the estimates of global error for cracked panel ($p = 2$, 32 elements)

| Number of increments | Estimated global error | | Global effectivity index | |
|---|---|---|---|---|
| | With balancing | Without balancing | With balancing | Without balancing |
| 1 | 0.948095(−1) | 0.790096(−1) | 0.838555 | 0.698810 |
| 2 | 0.107495(0) | 0.904738(−1) | 0.950753 | 0.800207 |
| 3 | 0.111550(0) | 0.980423(−1) | 0.986618 | 0.867148 |
| 4 | 0.113117(0) | 0.100715(0) | 1.000478 | 0.890787 |
| 5 | 0.114017(0) | 0.104075(0) | 1.008438 | 0.920505 |
| True value | 0.113063(0) | 0.113063(0) | 1.000000 | 1.000000 |

$$
\begin{aligned}
&-\varepsilon\,\Delta u_1 + x\,\frac{\partial u_1}{\partial x} - y\,\frac{\partial u_1}{\partial y} + xyu_1 - u_2 = 0\,,\\
&-\varepsilon\,\Delta u_2 + x\,\frac{\partial u_2}{\partial x} - y\,\frac{\partial u_2}{\partial y} - xyu_1 + u_2 = 0 \quad \text{in } \Omega\,,
\end{aligned}
\tag{52}
$$

where $\varepsilon = 1/100$, subject to the boundary conditions

$$
u_1 = \exp[(x^2 - y^2 - 1)/\varepsilon]\,, \qquad u_2 = xy\exp[(x^2 - y^2 - 1)/\varepsilon] \quad \text{on } \Gamma_D, \tag{53}
$$

and

$$
\begin{aligned}
\varepsilon\,\frac{\partial u_1}{\partial n} &= \varepsilon \boldsymbol{n}\cdot\nabla \exp[(x^2 - y^2 - 1)/\varepsilon]\,,\\
\varepsilon\,\frac{\partial u_2}{\partial n} &= \varepsilon \boldsymbol{n}\cdot\nabla xy\exp[(x^2 - y^2 - 1)/\varepsilon] \quad \text{on } \Gamma_N\,,
\end{aligned}
\tag{54}
$$

where $\Omega$, $\Gamma_D$ and $\Gamma_N$ are shown in Fig. 8.

The true solution to this problem is given by

$$
u_1 = \exp[(x^2 - y^2 - 1)/\varepsilon]\,, \qquad u_2 = xy\exp[(x^2 - y^2 - 1)/\varepsilon]\,. \tag{55}
$$

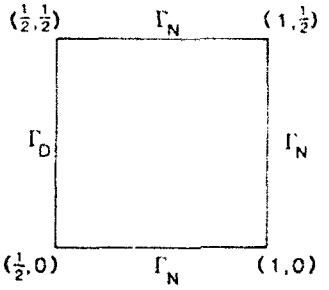


Fig. 8. Geometry and boundary conditions for unsymmetric elliptic system

The main feature of the solution is the presence of a strong boundary layer effect along the right-hand wall of the domain caused by the non-constant convection dominated flow field $\boldsymbol{b} = (x, -y)$.

In this case, the bilinear form $B(\cdot, \cdot)$ is unsymmetric. We choose the bilinear form $a(\cdot, \cdot)$ to be

$$a(\boldsymbol{u}, \boldsymbol{v}) = \int_\Omega (\varepsilon \nabla u_1 \cdot \nabla v_1 + \varepsilon \nabla u_2 \cdot \nabla v_2 + u_1 v_1 + u_2 v_2)\, \mathrm{d}\boldsymbol{x}\,. \tag{56}$$

The theory presented in [6] shows that the error estimator bounds the true error measured in the symmetrized norm. For the purposes of illustration, in this example we compute the true error in the symmetrized norm explicitly. It is this quantity which is labelled as the true error in Table 11.

The presence of the boundary layer indicates that an adaptive finite element analysis based on refining the mesh and enriching the degree of the approximation is suitable. The sequence of meshes generated during the analysis is shown in Figs. 9, 12, 15, 18 and 20. The meshes are not only irregular but contain elements of differing polynomial degree. The final mesh contains elements of degree six near the boundary layer. Nevertheless, the behaviour of the error estimator remains highly satisfactory as shown by the results in Table 11.

One source of concern when estimating errors for this type of problem is that the distribution of the estimated error will not agree with the distribution of the true error owing to the convective effect. Therefore, in Figs. 9–23, we present plots showing the distribution of the true and estimated errors. It is observed that the distribution of the estimated error closely reflects the actual error distribution.

Table 11
Behaviour of error estimators for unsymmetric elliptic system

| Mesh number | Degrees of freedom | True global error | Estimated global error | | Global effectivity index | |
|---|---|---|---|---|---|---|
| | | | With balancing | Without balancing | With balancing | Without balancing |
| 1 | 25 | 0.400129(0) | 0.420103(0) | 0.420218(0) | 1.049919 | 1.050206 |
| 2 | 51 | 0.145063(0) | 0.144794(0) | 0.147063(0) | 0.998146 | 1.013787 |
| 3 | 111 | 0.563992(−1) | 0.564022(−1) | 0.564159(−1) | 1.000053 | 1.000296 |
| 4 | 165 | 0.646845(−2) | 0.647644(−2) | 0.649044(−2) | 1.001235 | 1.003400 |
| 5 | 340 | 0.263345(−2) | 0.272907(−2) | 0.274071(−2) | 1.036310 | 1.040730 |

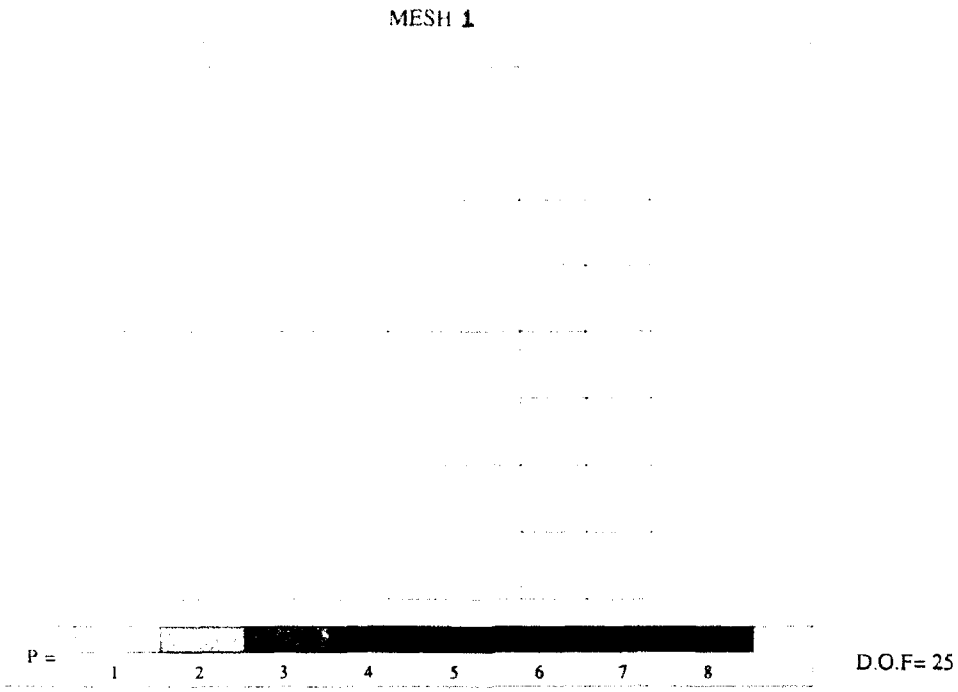


Fig. 9. Adaptive analysis of unsymmetric elliptic system. Mesh 1.

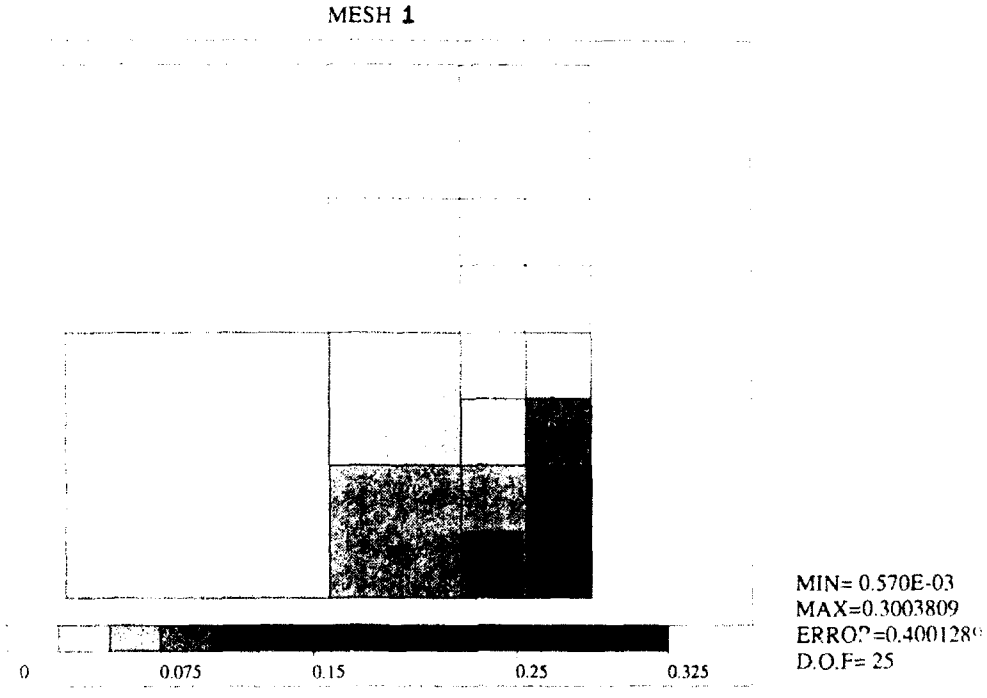


Fig. 10. Adaptive analysis of unsymmetric elliptic system. Distribution of true error on Mesh 1.

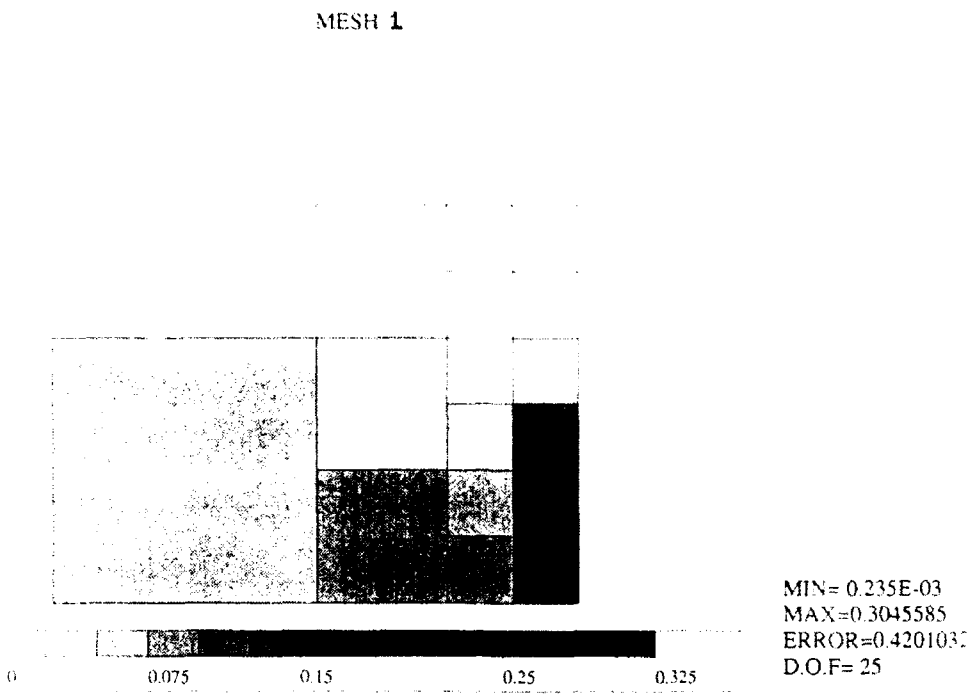


Fig. 11. Adaptive analysis of unsymmetric elliptic system. Distribution of estimated error on Mesh 1.

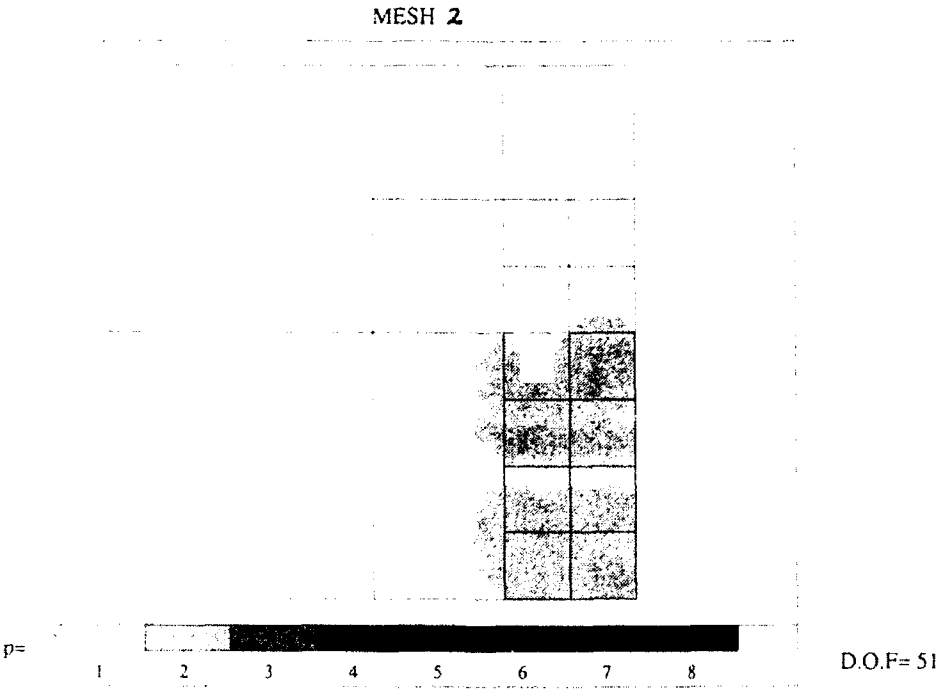


Fig. 12. Adaptive analysis of unsymmetric elliptic system. Mesh 2.

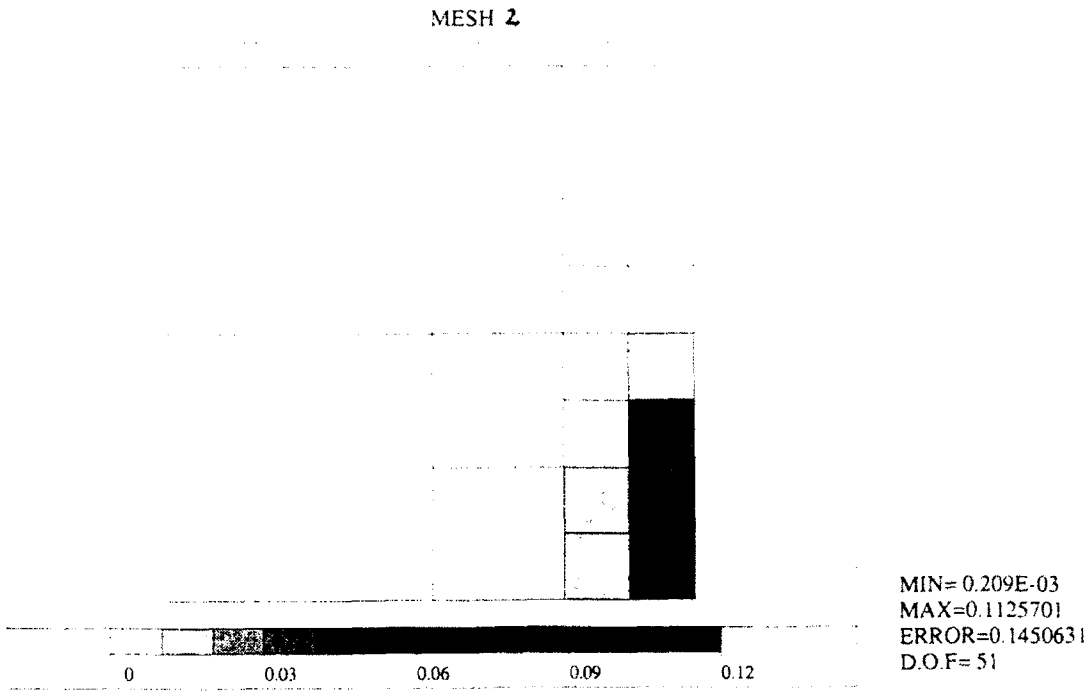


Fig. 13. Adaptive analysis of unsymmetric elliptic system. Distribution of true error on Mesh 2.

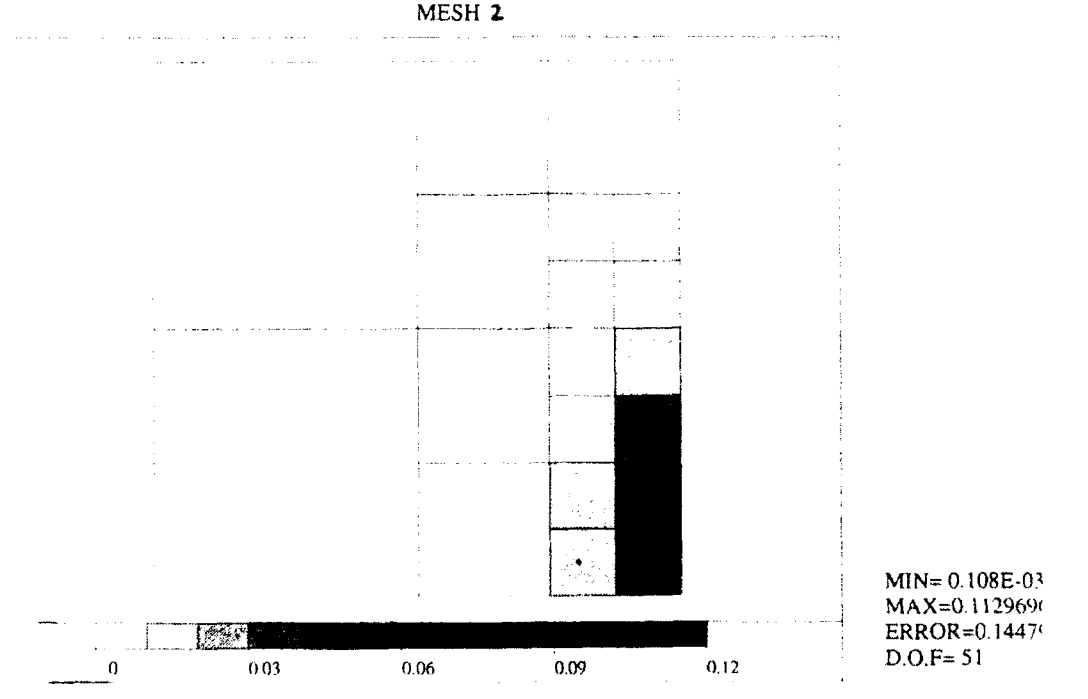


Fig. 14. Adaptive analysis of unsymmetric elliptic system. Distribution of estimated error on Mesh 2.

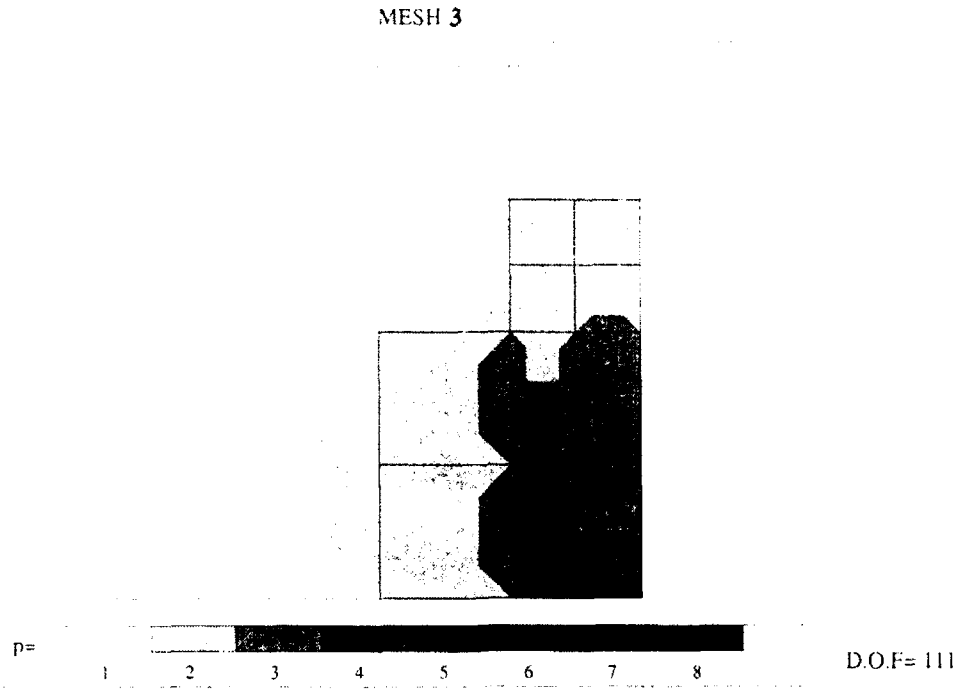


Fig. 15. Adaptive analysis of unsymmetric elliptic system. Mesh 3.

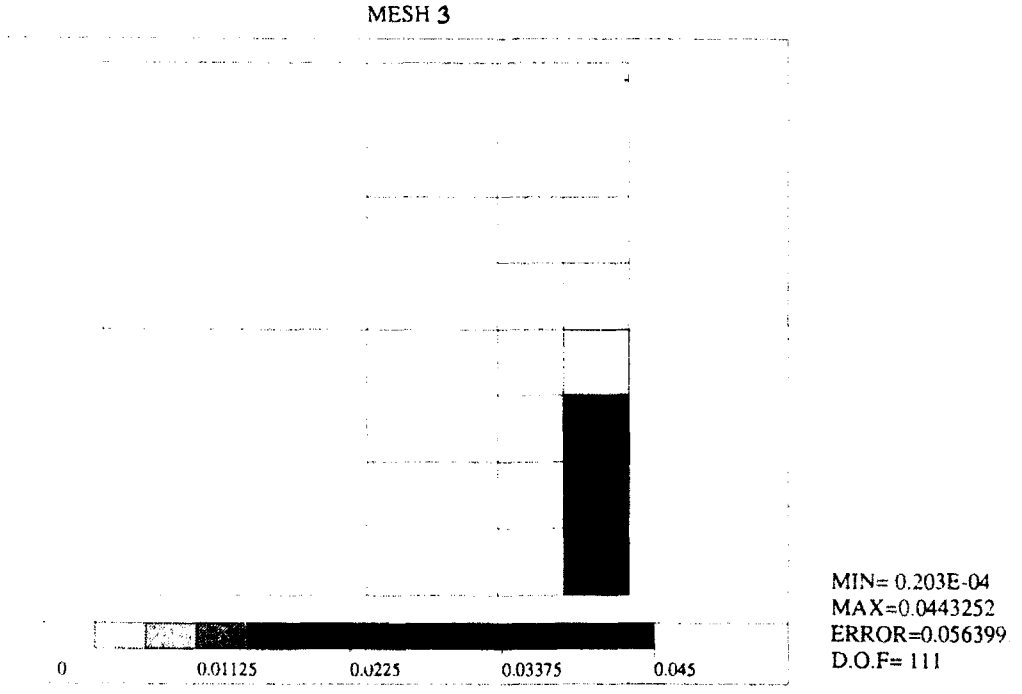


Fig. 16. Adaptive analysis of unsymmetric elliptic system. Distribution of true error on Mesh 3.

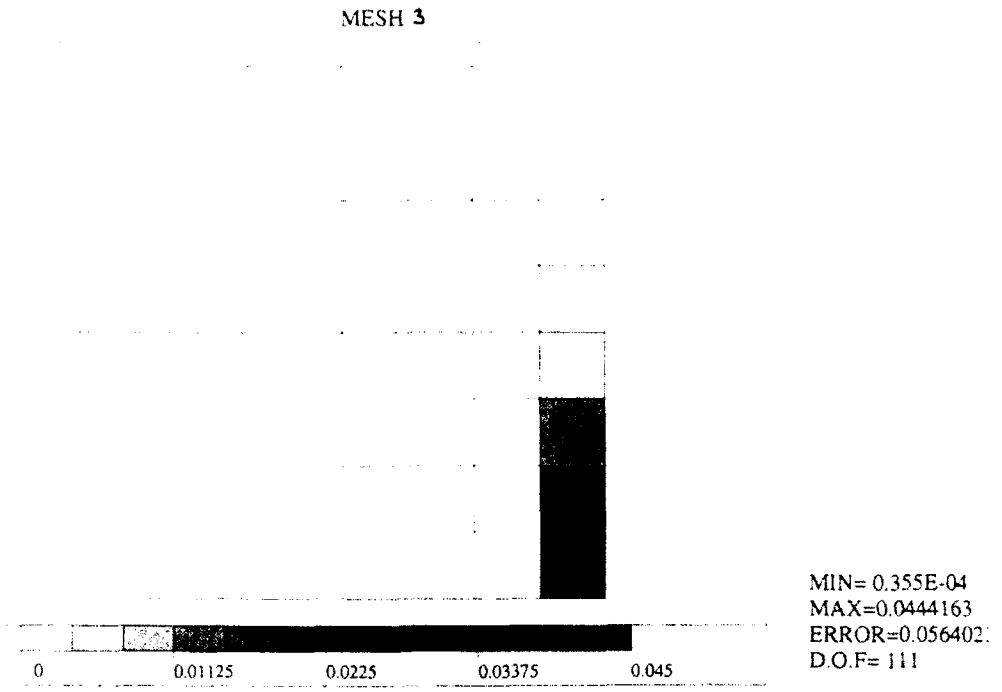


Fig. 17. Adaptive analysis of unsymmetric elliptic system. Distribution of estimated error on Mesh 3.

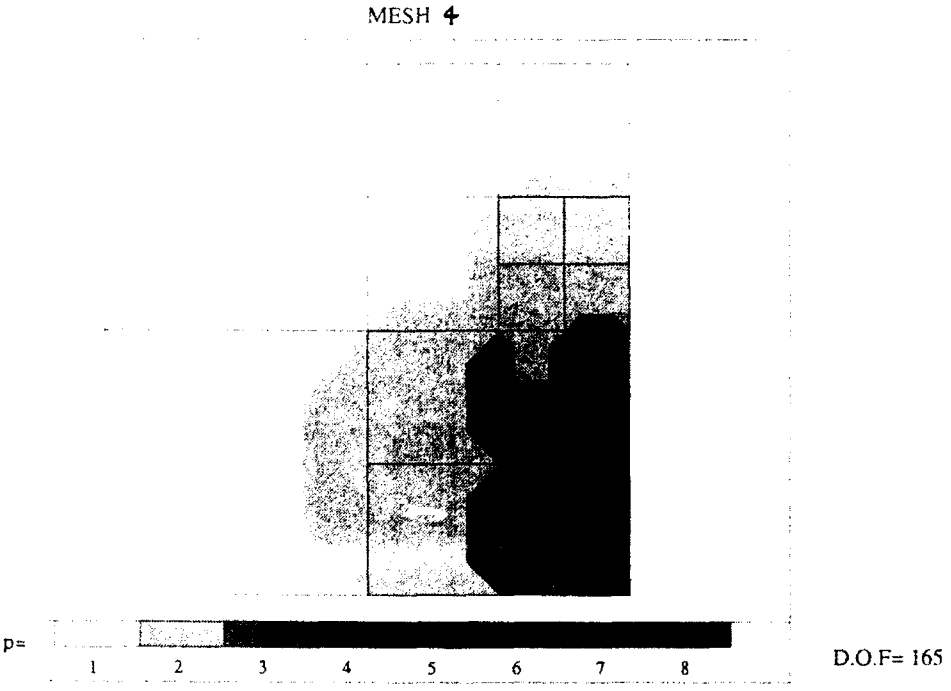


Fig. 18. Adaptive analysis of unsymmetric elliptic system. Mesh 4.

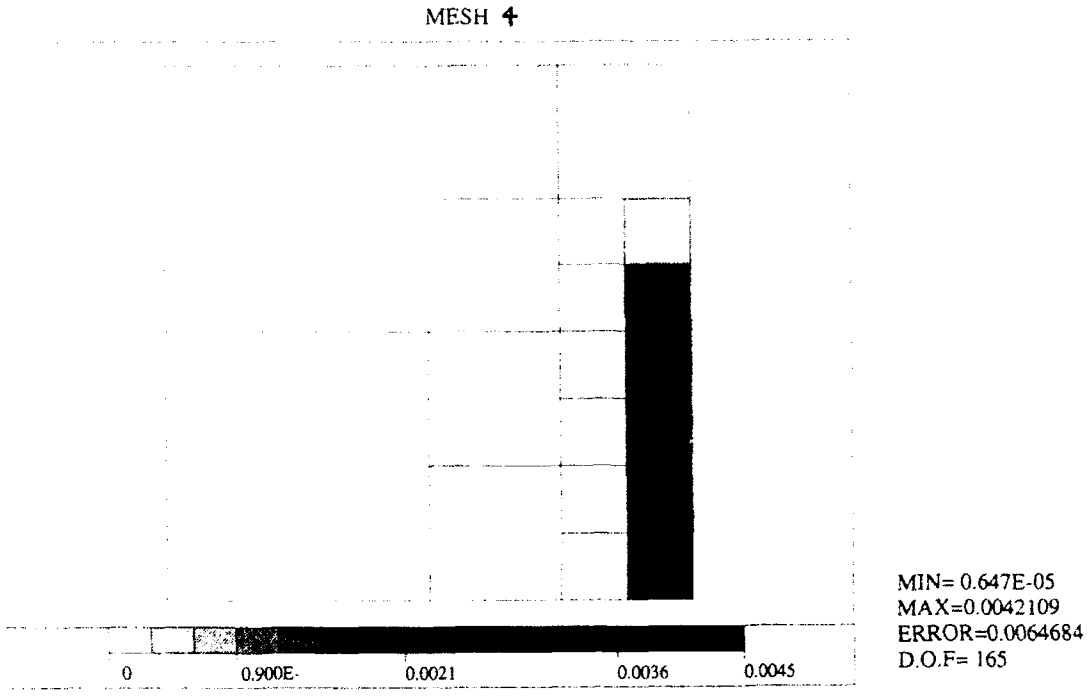


Fig. 19. Adaptive analysis of unsymmetric elliptic system. Distribution of true error on Mesh 4.

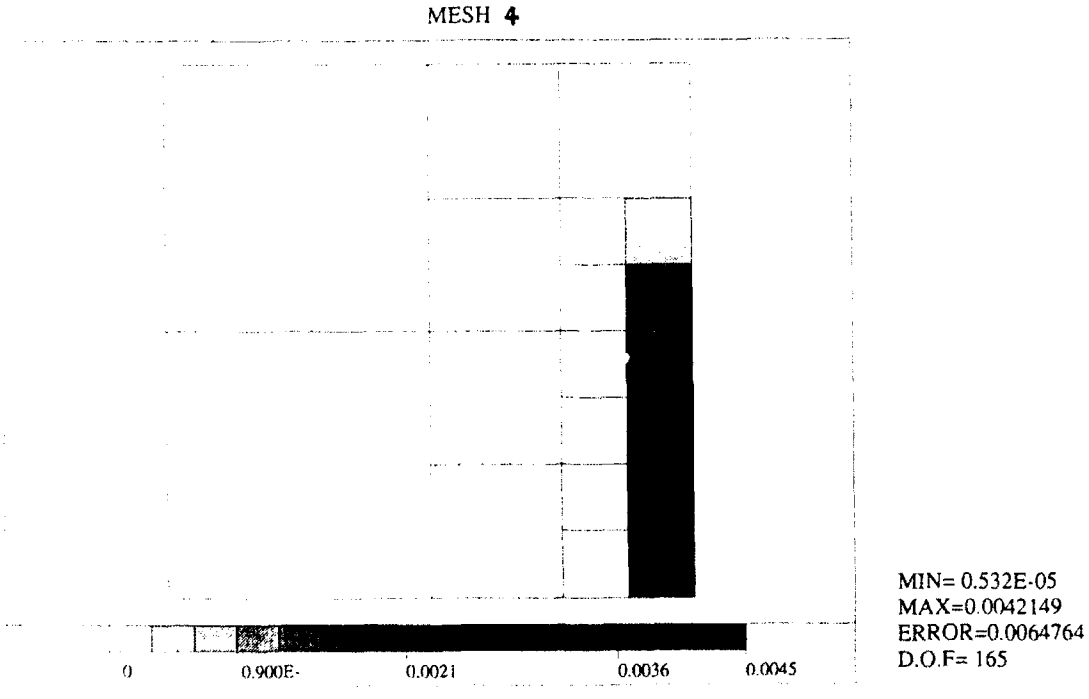


Fig. 20. Adaptive analysis of unsymmetric elliptic system. Distribution of estimated error on Mesh 4.

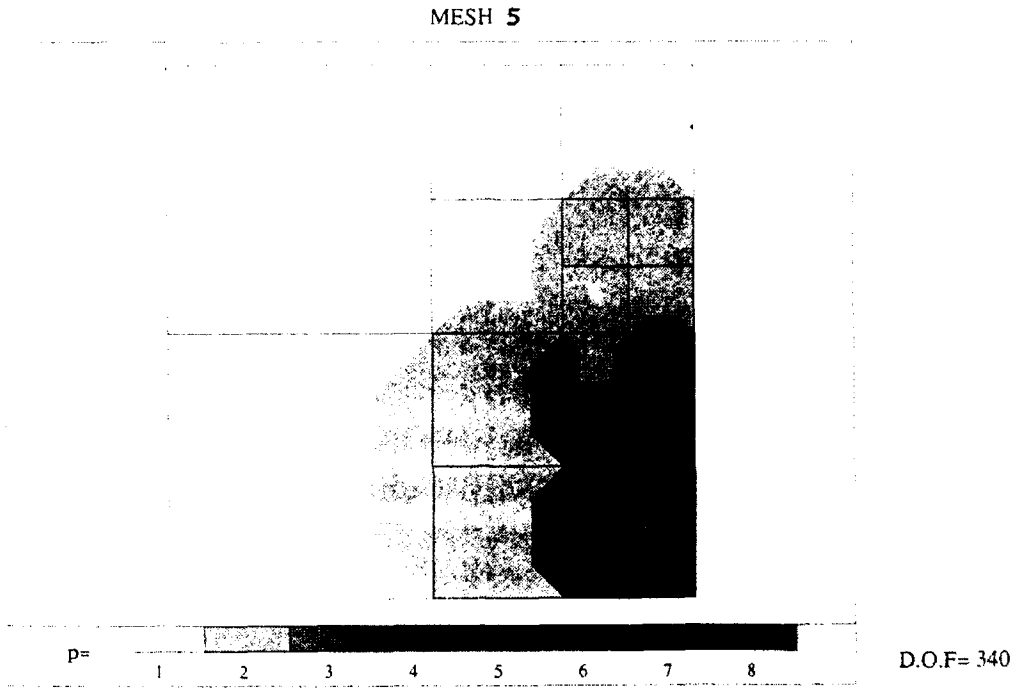


Fig. 21. Adaptive analysis of unsymmetric elliptic system. Mesh 5.

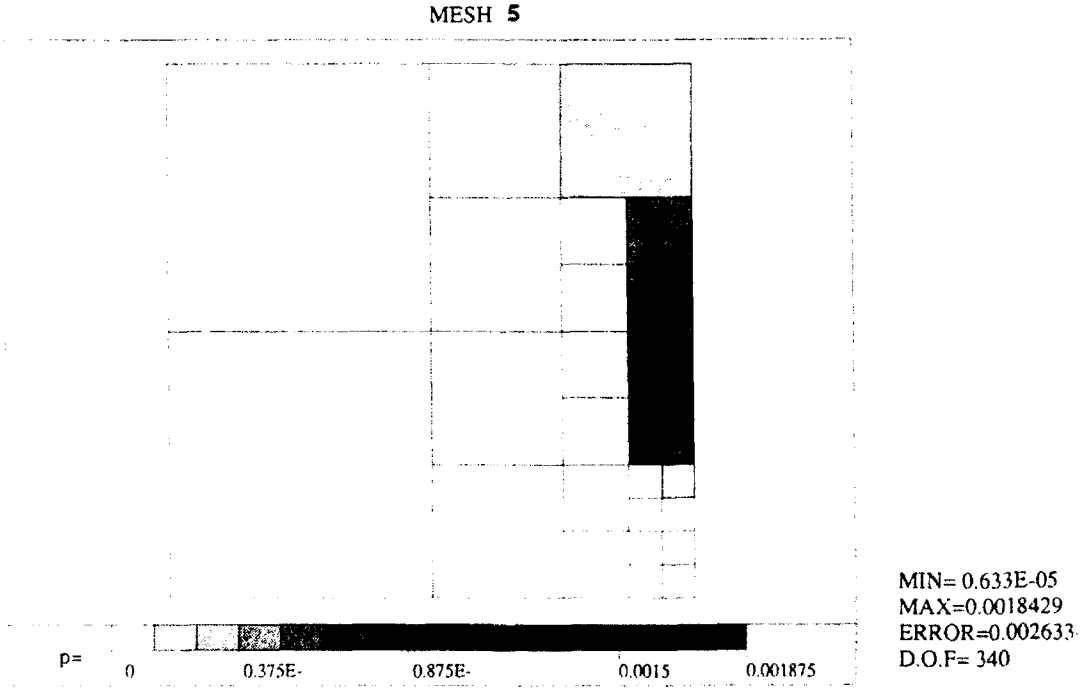


Fig. 22. Adaptive analysis of unsymmetric elliptic system. Distribution of true error on Mesh 5.

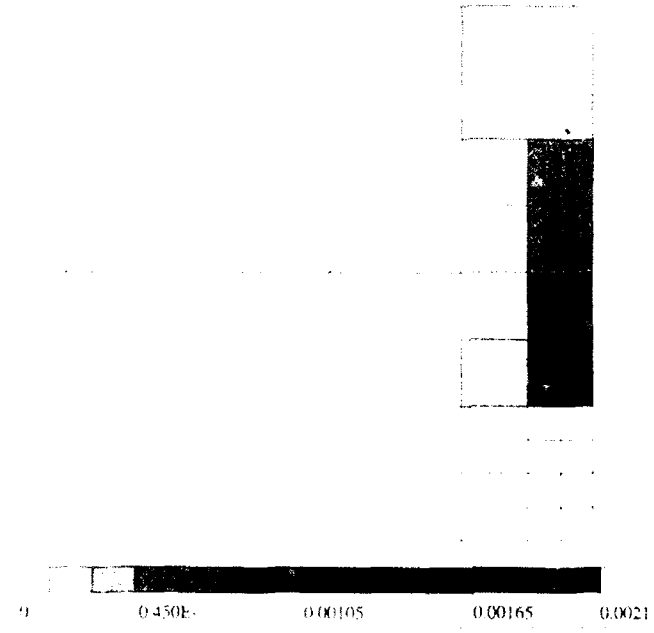






Fig. 23. Adaptive analysis of unsymmetric elliptic system. Distribution of estimated error on Mesh 5.

## Acknowledgment

The support of this work by ONR under grant N00014-89-J-1451, NSF under grant ASC-9111540 and ARO under contract DAAL03-89-K-0120 is gratefully acknowledged.

## References

[1] M. Ainsworth and J.T. Oden, A unified approach to a posteriori error estimation based on element residual methods, unpublished.

[2] R.E. Bank and A. Weiser, Some a posteriori error estimators for elliptic partial differential equations, Math. Comp. 44 (1985) 283–301.

[3] J.T. Oden, L. Demkowicz, T.E. Strouboulis and Ph. Devloo, Adaptive methods for problems in solid and fluid mechanics, in: I. Babuška, O.C. Zienkiewicz, J. Gago and E.R. de A. Oliveira, eds., Accuracy Estimates and Adaptive Refinements in Finite Element Computations (Wiley, New York, 1986) 249–280.

[4] D.W. Kelly, The self equilibration of residuals and complementary error estimates in the finite element method, Internat. J. Numer. Methods Engrg. 20 (1984) 1491–1506.

[5] J.T. Oden, L. Demkowicz, W. Rachowicz and T.A. Westermann, Towards a universal *h-p* finite element strategy, Part 2. A posteriori error estimation, Comput. Methods Appl. Mech. Engrg. 77 (1989) 113–180.

[6] M. Ainsworth and J.T. Oden, A posteriori error estimators for second order elliptic systems. Part 1. Theoretical foundation and a posteriori error analysis, Computers in Mathematics and Applications (in press).

[7] J.T. Oden, L. Demkowicz, W. Rachowicz and T.A. Westermann, A posteriori error analysis in finite elements: The element residual method for symmetrizable problems with applications to compressible Euler and Navier–Stokes equations, Comput. Methods Appl. Mech. Engrg. 82 (1990) 183–203.

[8] M. Ainsworth and J.T. Oden, A posteriori error estimators for second order elliptic systems. Part 2. An optimal order process for calculating self equilibrating fluxes, Computer in Mathematics with Applications (in press).

[9] I. Babuška and W.C. Rheinboldt, A posteriori error estimates for adaptive finite element computations, SIAM J. Numer. Anal. 15 (1978) 736–754.